PAPER

Check for updates

Stable tandem luminescent solar concentrators based on CdSe/CdS quantum dots and carbon dots†

Guiju Liu, Haiguang Zhao, [ID]* Feiyu Diao, Zhibin Ling and Yiqian Wang*

Luminescent solar concentrators (LSCs) serve as large-area sunlight collectors, which are suitable for applications in semi-transparent, low-cost photovoltaics. Colloidal quantum dots (QDs) are promising candidates as a new type of absorber/emitter in LSCs, due to their size-tunable wide absorption spectrum, narrow emission spectrum, high quantum yield and structure-engineered large Stokes shift. However, due to the lack of long-term photo-stability of QDs, it is still a challenge to prepare photostable LSCs. Compared with colloidal QDs, carbon dots (C-dots) exhibit excellent photo-stability, presenting a very promising solution to improve the long-term photo-stability of quantum dot based LSCs. Here, as a proof-of-concept, we report the enhancement of the photo-stability of LSCs based on CdSe/CdS QDs by using a tandem structure of LSCs. We fabricated a large-area ($\sim$100 cm^2) thin film and placed this thin film on the top of a luminescent solar concentrator (LSC) based on CdSe/CdS QDs. The as-fabricated semi-transparent tandem device exhibits an external optical efficiency of $\sim$1.4% under one sun illumination, which is a 16% enhancement in the efficiency over the LSC based on CdSe/CdS QDs. More importantly, the presence of C-dots largely enhances the photo-stability of the LSC device based on CdSe/CdS QDs under ultraviolet (UV) illumination. After 70 hour UV illumination, the QD-based LSC with a protective layer of C-dot thin film retains 75% of its initial integrated photoluminescence intensity, which is 1.8 times higher than that of the LSC without the C-dot layer. Our work indicates that C-dots can be used as an additional layer in LSCs to enhance both the efficiency and long-term photo-stability.

1. Introduction

Solar technologies, such as solar cells and water splitting for fuel production, offer a promising opportunity to solve the currently increasing demand for renewable energy.[1–3] Current commercial solar cells such as Si wafer-based and CuIn$_x$Ga$_{1-x}$Se$_2$ photovoltaics (PVs) exhibit not only a high power conversion efficiency (PCE) of over 20%, but also long-term stability, with only 20% decrease in the PCE after outdoor use for 20 years.[4–8] However, the cost of solar electricity generated by commercial solar cells (*e.g.* silicon solar cells, thin film solar cells) is still quite high.[9] In recent years, low-cost and solution-processing excitonic (electron–hole pair) solar cells, such as organic (*e.g.* dye or polymer), quantum dots (QDs) and perovskite PVs have emerged.[10–15] For example, hybrid organic–inorganic perovskite PVs exhibit a PCE of over 20%, but so far this type of solar cell is not very stable during outdoor cell operation because the

perovskite material is easily degraded.[15] Another potential technology to achieve cost-effective electricity is to use luminescent solar concentrators (LSCs).[16–22] LSCs can be used as low-cost large-area sunlight collectors for PVs, which can not only decrease the cost of electricity by reducing the use of PV materials (*e.g.* c-Si), but also enhance the response of PVs to diffused light.[16–22] Such devices are flexible in their design, because of their shape/color tenability, making them easily integrated into buildings or appliances. Typically, a luminescent solar concentrator (LSC) consists of an optical waveguide embedded with highly emissive fluorophores.[16–22] After the absorption of sunlight, QDs re-emit photons at a longer wavelength range and these photons are guided towards the PVs positioned at the edges of the LSC due to total internal reflection. The concentrated photons are converted to electricity by a solar cell coupled to the edges of the LSC.[18,19]

Initially, the luminescent species in the optical waveguide are mainly organic dye molecules, but the performance of these LSCs is limited by the poor stability of the dyes and the large reabsorption energy losses due to their significant overlap of the absorption and emission.[16,17] Quite recently, colloidal semiconductor nanocrystals [*e.g.* QDs such as CdSe/CdS and

College of Physics & State Key Laboratory, Qingdao University, No. 308 Ningxia Road, Qingdao 266071, People's Republic of China. E-mail: hgzhao@qdu.edu.cn, yqwang@qdu.edu.cn

PbS/CdS, inorganic perovskites, and carbon dots (C-dots)] have been used as efficient emitters in LSCs due to their high photoluminescence quantum yield (PL QY), size/chemical composition tunable wide absorption spectrum (300–1000 nm), and solution processability.[19–22] More importantly, the Stokes shift (energy gap between the first-absorption peak and emission peak) of QDs can be engineered to be very large, which is a key parameter to realize large-area high efficiency LSCs as the spectral overlap often leads to a reabsorption energy loss.[21–23] Typically, the available approaches so far to engineer the Stokes shift include doped QDs (e.g. Mn doped ZnSe),[24] heterostructured QDs (e.g. PbS/CdS,[20] CdSe/CdS[21,22]), intra-gap QDs (e.g. CuInSSe[25,26]) and indirect band gap QDs (e.g. Si).[27] For example, LSCs based on core/shell CdSe/CdS QDs exhibit an external optical efficiency (η, the ratio of the optical power of re-emitted photons on the edges over the optical power of incident photons on the top) of 1% with a lateral size of 1.5×20 cm^2 benefiting from their high PL QY of 40% and large Stokes shift of 400 meV.[22] Although the PL QY (40%) is lower than the typical PL QY of organic dyes, the obtained PL QY is still relatively high for the group of QDs. In order to increase the optical efficiency of LSCs, another efficient approach is to use multiple stacked waveguides.[16,17,28,29] For example, a total optical efficiency of up to 4% has been reported for a stack of two LSC plates, one being coupled to a GaAs solar cell, and the other to a Si solar cell.[28] Desmet et al.[29] also investigated the stacking of LSCs with traditional organic dyes and a perylene perinone dye, and obtained an efficiency of 4.2%. Very recently, tandem LSCs based on two types of QDs with tunable absorption were fabricated, in which each layer is designed to absorb different portions of the solar spectrum. The tandem LSCs exhibit a considerable boost in the efficiency compared to single-layer devices.[30]

Besides great research efforts focusing on the enhancement of efficiency in LSCs, the long-term stability of LSCs is an important consideration for the lifetime of such devices. For conventional benchmark systems, researchers have made an effort to enhance the stability of LSCs by choosing appropriate fluorophores (perylene-based organic luminescent dyes)[31] or waveguide host materials (e.g. crosslinked fluorinated polymers and organic–inorganic hybrid waveguides).[32–34] Meanwhile, for LSCs based on semiconductor nanocrystals (e.g. colloidal bare QDs or core/shell QDs, quantum wells and perovskites), researchers have mainly focused on selecting various fluorophore nanocrystals to enhance the stability of the devices.[19,20,35,36] Usually, colloidal QDs are capped with organic ligands, which not only endow the QDs with colloidal stability in solution, but also passivate the surface atoms of the QDs.[19,20,23] Efficient surface passivation can largely decrease the number of quantum dot (QD) surface defects/traps, which can not only largely enhance the PL QY, but also decrease the emission in the long wavelength range due to the trapping of emission.[37,38] In addition, surface defects/traps usually serve as surface active centers to accelerate the QD surface oxidation or degradation when QDs are exposed to ultraviolet (UV) light.[38] Typically, LSCs based on QDs are required to exhibit stable optical properties, such as PL QY, photoluminescence (PL) peak shape and optical transparency when they are exposed to harsh

environmental conditions such as high humidity, UV light and high temperature (up to 100 °C).[18,25] LSCs can be sealed with glass, which can isolate LSCs from humidity and air (oxygen), but the QDs still suffer from light-induced degradation under sunlight (mainly UV light), which leads to both the decrease of the PL QY and the variation of the PL peak/shape.[25] For example, Klimov's group used core/thick-shell CdSe/Cd$_{0.6}$Zn$_{0.4}$S QDs with or without silica coating for LSCs.[25] They found that the bare QDs retained only 23% and the silica-coated QDs retained 85% of the original PL QY after illumination for 4 months (room light in air).[25] Zhou et al.[19] found that the PL intensity of an LSC based on core/thick-shell CdSe/CdPbS QDs retains 90% of its initial PL QY after a 12 h test (400 nm light emitting device with an intensity of 1.3 W cm^{-2}) under ambient conditions.

In stark contrast to the environmental sensitivity of QDs, some C-dots exhibit excellent PL stability under UV light in ambient conditions.[19] Also, the synthesis/purification/post-use process of C-dots does not require any gas protection (N$_2$ or Ar) against surface oxidation. In stark contrast, the synthesis of high-quality inorganic QDs requires gas protection.[19,39–41] Typically, C-dots are synthesized using a solvothermal approach.[40,41] Recently, there were some reports on C-dots or their hybrids with inorganic materials embedded in an appropriate matrix or prepared as solid macrostructures to improve the optical properties and stability of the optical devices.[42–46] Quite recently, C-dot based LSCs were prepared by casting C-dots on a glass substrate.[19,47] For example, an LSC based on C-dots (dimensions: 10×10 cm^2) could exhibit larger η (1.1%) and better PL photo-stability compared to LSCs based on inorganic QDs.[19]

Here we demonstrate the preparation of a tandem LSC, which consists of two layers, the top layer being an LSC based on C-dots, and the bottom layer being an LSC based on CdSe/CdS QDs. The C-dot layer serves as a protective layer to improve the photo-stability of the bottom layer of the LSC based on CdSe/CdS. We firstly synthesized C-dots, which absorb sunlight in the broad UV region (300–550 nm). Then a C-dot/polyvinyl-pyrrolidone (PVP) mixture in methanol was spin-coated on a glass substrate. As a proof-of-concept, we incorporated CdSe/CdS QDs into a poly(lauryl methacrylate-co-ethylene glycol dimethacrylate) (PLMA-co-EGDA) polymer matrix to fabricate LSCs with dimensions of 10×10 cm^2. The top layer LSC based on C-dots not only enhances the η of the LSC based on CdSe/CdS QDs, but also largely improves its photo-stability under UV illumination (400 nm light emitting device with an intensity of 1.3 W cm^{-2}). These results indicate that C-dots are an excellent candidate as a highly-stable protective layer for improving the photo-stability of inorganic QD based LSCs.

2. Experimental section

2.1. Synthesis of the QDs

CdSe QDs were synthesized by using a hot injection approach and subsequently, a successive ionic layer adsorption and reaction (SILAR) method was used to synthesize CdSe/CdS QDs.[23] The as-synthesized QDs were dispersed in hexane for

further synthesis of core/shell CdSe/CdS QDs *via* a SILAR approach.[23] Typically, Cd(OA)$_2$ and S were used as precursors in the presence of oleylamine and oleic acid as capping ligands. The as-prepared CdSe/CdS QDs with thirteen monolayers of CdS shell were dispersed in toluene for further fabrication of LSCs. The full description of the synthetic approach is presented in the ESI.†

2.2. Synthesis of C-dots

C-dots were prepared *via* a hydrothermal approach.[41] Typically, 1 g citric acid and 2 g urea in 10 mL dimethylformamide were reacted for 6 h at 160 °C in an autoclave. The mixture was further treated with NaOH aqueous solution (50 mg mL^{-1}).[41] Then the mixture was transferred into dialysis bags (3000 Da) for 2 h. The mixture inside the dialysis bag was collected. The detailed synthetic approach is presented in the ESI.†

2.3. Preparation of the LSCs

The thin film LSC based on C-dots was prepared by following the reported literature using a spin coating appraoch.[19] Typically, a C-dot/PVP polymer mixture in methanol with a final concentration of PVP of 200 mg mL^{-1} and C-dots of 15 mg mL^{-1} were spin-coated on a glass substrate at a speed of 500 rpm and an acceleration of 800 rpm per s for 60 s.[19] PLMA polymer based LSCs using CdSe/CdS QDs as the emitters were prepared by embedding the QDs in the polymer matrix.[23] The detailed approach is shown in the ESI.†

2.4. Characterization

X-ray diffraction (XRD) analysis was performed on a Philips X'pert diffractometer using a Cu-Kα radiation source (λ = 0.15418 nm). The transmission electron microscopy (TEM) examination of the QDs was carried out using a JEOL JEM2100F TEM equipped with an energy dispersive X-ray spectrometer (EDS). A UV-2600 UV-vis spectrophotometer (Shimadzu) with a scan speed of 600 nm min^{-1} was used to obtain the absorption spectra of the investigated samples. Fluorescence spectra were acquired using an FLS980 instrument (Edinburgh) without any mirror or scattering layer on the bottom of the LSC. The PL lifetimes of the C-dots and the CdSe/CdS QDs in the polymer matrix before and after UV illumination were measured using pulsed laser diodes of 350 nm (C-dots) and 440 nm (CdSe/CdS QDs) using the time-correlated single photon counting (TCSPC) mode in the FLS980 system. The PL QY of the C-dots or the CdSe/CdS QDs was measured by using Rhodamine 6G as a reference. The external optical efficiency of the LSCs was measured by using a solar simulator at AM 1.5G (100 mW cm^{-2}). During the measurements, the power meter (Newport Model 843-R) was directly coupled on one side of the LSC edges without using any optical devices (Fig. S1, ESI†). For the tandem LSC, the LSC based on the C-dots is placed on the top of the LSC based on the QDs. The air gap between the LSCs is around 1 cm, which is the optimal distance for the highest external optical efficiency. The overall efficiency of the tandem LSC is the sum of the efficiencies of the two individual LSCs. More details are given in the ESI.† For stability measurements, the PL intensity of the LSCs was measured by PL spectroscopy upon UV illumination (a 400 nm light emitting device with an intensity of 1.3 W cm^{-2} measured using an optical power meter) under ambient conditions (a temperature of 25 °C and a humidity of 40%).[19]

3. Results and discussion

3.1. Synthesis of the C-dots and the CdSe/CdS QDs

C-dots were prepared *via* a hydrothermal approach.[19,41] The as-synthesized C-dots were further treated with NaOH to decrease the absorption in the long wavelength range.[41] The Na$^+$ capped C-dots dispersed in methanol or water exhibit a PL QY of 40 ± 5%, which is 30 ± 5% higher than that of the untreated C-dots due to the improvement of surface passivation. The colloidal CdSe/CdS QDs dispersed in hexane exhibit a typical PL QY of 50 ± 5%.

XRD patterns were used to elucidate the crystalline phases of the synthetic materials (Fig. S2, ESI†). A broad peak can be observed at around $2\theta = 25°$ for the C-dots (Fig. S2a, ESI†), corresponding to the highly disordered carbon atoms.[48] The CdSe QDs have a zinc-blend (ZB) structure, which is the typical phase of the CdSe QDs grown at 300 °C. When covered with the CdS shell, the structure of the QDs exhibits a wurtzite (WZ) structure (Fig. S2b, ESI†). The structure of these QDs can be further confirmed using the TEM images. Fig. 1a illustrates that the C-dots are spherical and well dispersed, and the C-dots range from 2 nm to 6 nm in diameter (Fig. 1b). The inset in Fig. 1a shows a high-resolution TEM (HRTEM) image of an individual C-dot with a lattice spacing of 3.26 Å, corresponding to the (002) plane of the graphitic carbon. As shown in Fig. 1c and e, the CdSe and CdSe/CdS QDs have highly crystalline microstructures. The inset in Fig. 1c displays a typical HRTEM image of one CdSe QD and the lattice spacing is measured to be 3.12 Å and 3.49 Å with an angle of 54.74° between the two planes, which is associated with the (200) and (11$\bar{1}$) planes of the ZB CdSe material, suggesting that the particle is viewed along the [011] zone axis. The statistical analysis of the particle size for the CdSe QDs is shown in Fig. 1d, which demonstrates a high uniformity for the samples. After the growth of the 13 monolayers of CdS, the final diameter of the QDs increases from 3.32 nm (CdSe QDs) to 10.57 nm (CdSe/13CdS QDs) with a shell thickness of ~3.63 nm (Fig. 1d and f). The inset in Fig. 1e displays a typical HRTEM image of an individual CdSe/CdS QD viewed along the [011] zone axis. The measured lattice spacings of 3.21 Å and 3.25 Å are well consistent with the (0$\bar{1}$1) and (1$\bar{1}$1) planes of the WZ structure of CdS.[22,23] The EDS study reveals the presence of elemental Cd, Se and S, indicating the successful synthesis of the core–shell CdSe/CdS QDs (Fig. S3, ESI†).

3.2. Fabrication and optical properties of the LSCs

The as-prepared thin film LSC based on the C-dots has a lateral size of 10 × 10 cm^2.[19] By optimizing the concentration of the C-dots in PVP/methanol solution and the parameters of the spin-coating process, we can well control the thickness of the C-dot/PVP film, thus adjusting the degree of transparency of the as-fabricated thin film. Fig. 2a shows the PL spectra of
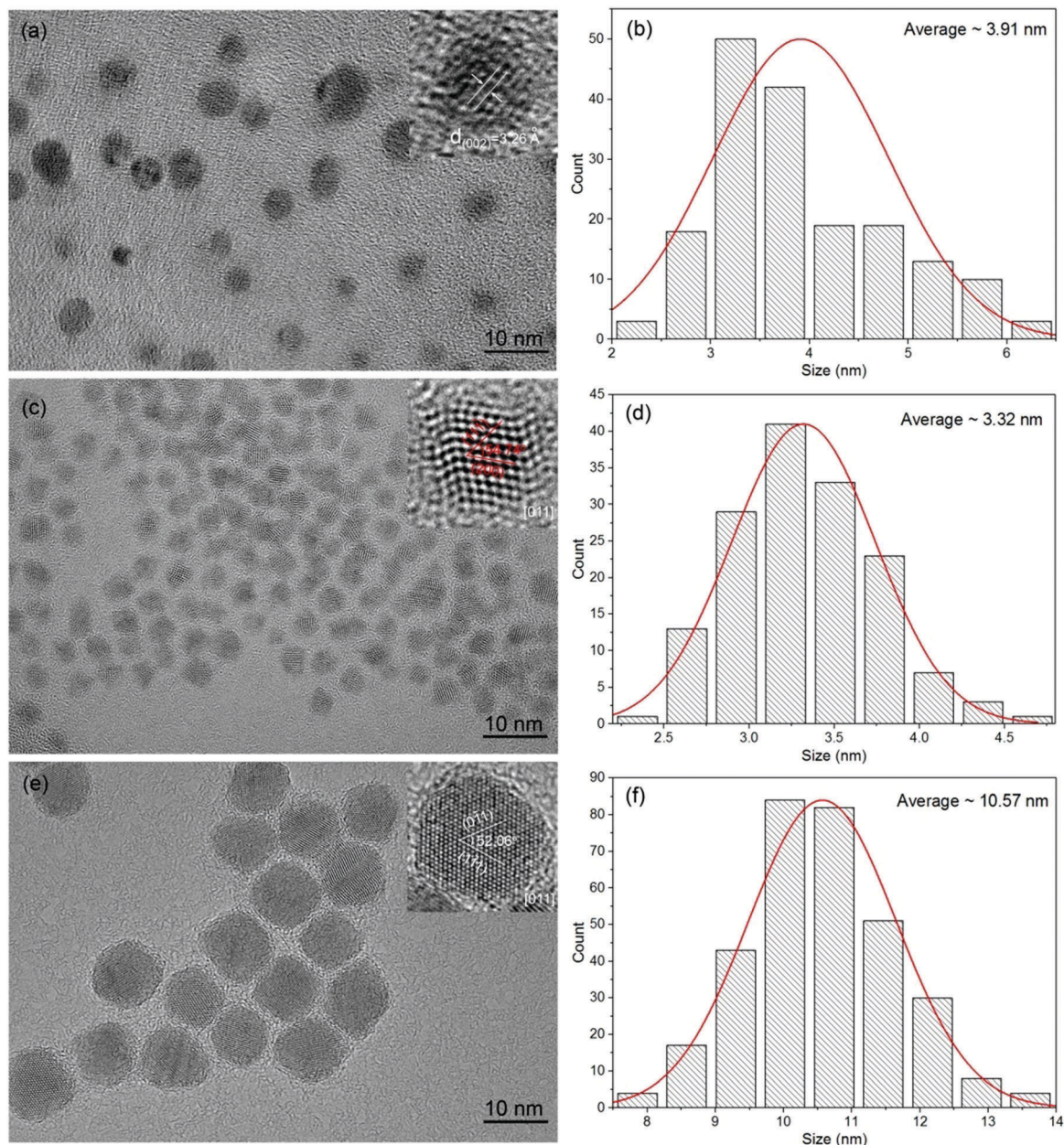
Fig. 1 Representative TEM images of C-dots (a), CdSe QDs (c) and CdSe/CdS QDs (e). The insets are the HRTEM images of individual particles. (b), (d) and (f) Size distribution of the C-dots, CdSe QDs and CdSe/CdS QDs. Red lines are the Gaussian fits of the experimental data.

the C-dot/PVP film with different C-dot weight percentages in PVP. The weight percentage of the C-dots is calculated by thermogravimetric analysis (TGA) (Fig. S4, ESI†). The PL intensity of the C-dot/PVP film at 520 nm increased with the stepwise addition of C-dot content under excitation at 390 nm. Then, the emission decreased as the C-dot content is further increased. As shown in Fig. 2b and Fig. S5 (ESI†), the PL intensity increases with the increase of the C-dot content (5–15 wt%), whereas when the C-dot concentration is further increased, the PL intensity undergoes a decrease. This behavior indicates that a high C-dot concentration may lead to PL quenching, which is similar to standard benchmark systems based on organic dyes.[49] Based on these analyses, the optimized C-dot content in PVP is ∼13 wt%.

In addition to the change in the PL intensity, a red-shift of the emission spectra is observed as the content of the C-dots is increased from 6.5 wt% to 37.4 wt%, which is due to the energy transfer. At the high weight percentage of C-dots in PVP (>15%), we did observe two emissions.[42,45] As there is no absorption/emission spectral overlap in the range of 550–600 nm (Fig. 3a), we exclude that the shoulder appeared in the emission profile in Fig. 2a results from reabsorption, which is different from that of an organic dye system.[50–52] We believe that this dual emission is due to the Förster energy transfer between the neighbor QDs as the concentration of the C-dots is very high.

The absorption and PL spectra of the optimized C-dot based LSCs and the C-dots in methanol are shown in Fig. 3a.
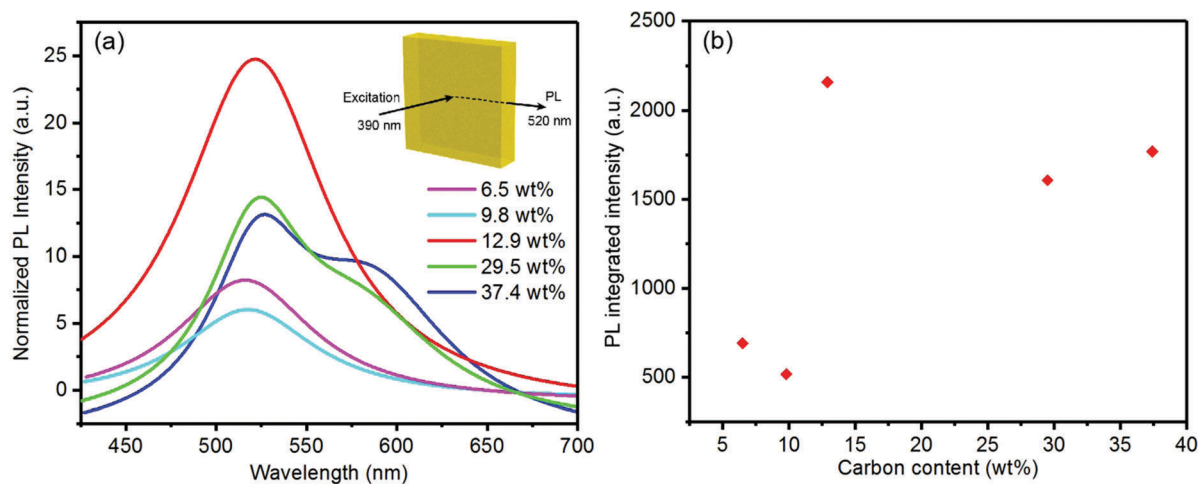
10062 | J. Mater. Chem. C, 2018, **6**, 10059–10066

This journal is © The Royal Society of Chemistry 2018

Fig. 2 (a) PL spectra (λ_{ex} = 390 nm) of C-dot/PVP with increasing C-dot content. The inset shows the excitation optical path diagram. (b) Plot of the integrated PL intensity as a function of the C-dot weight percentage in PVP measured by TGA.

The C-dots absorb in the entire UV wavelength range of 300–550 nm. There is a slight variation in the spectral range of 300–350 nm for the C-dots in methanol and in the LSCs due to the absorption of the PVP polymer (Fig. 3a and Fig. S6, ESI†). The maximum absorption at 350 nm is around 0.65, indicating that 80% of the UV light at this wavelength can be absorbed by the C-dot thin film ($A = -\lg T$, where A is the absorption, and T is the transmittance).[25] In the wavelength range of 400–500 nm, the maximum absorption at 460 nm is around 0.3, meaning that 50% of the light was absorbed by the C-dots. A typical Stokes shift of 250 meV was achieved for the as-synthesized C-dots, indicating a relatively small overlap between the absorption and emission spectra (Fig. S7, ESI†).[19] The C-dots dispersed in the PVP polymer have a PL QY of 40%, which shows no significant changes of PL QY for the C-dots in solution.

The LSCs based on colloidal QDs were fabricated by incorporating CdSe/CdS QDs into a PLMA matrix.[22] The dimensions
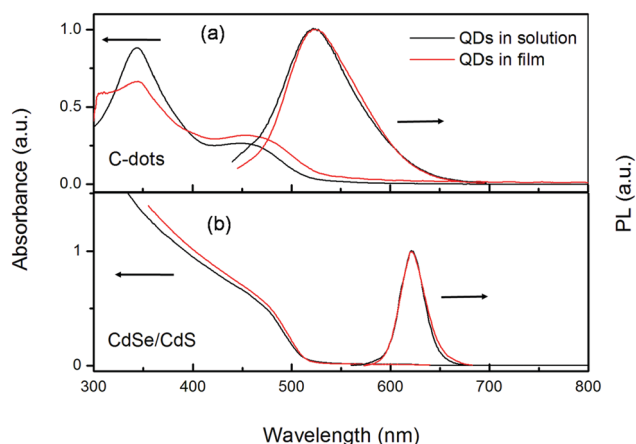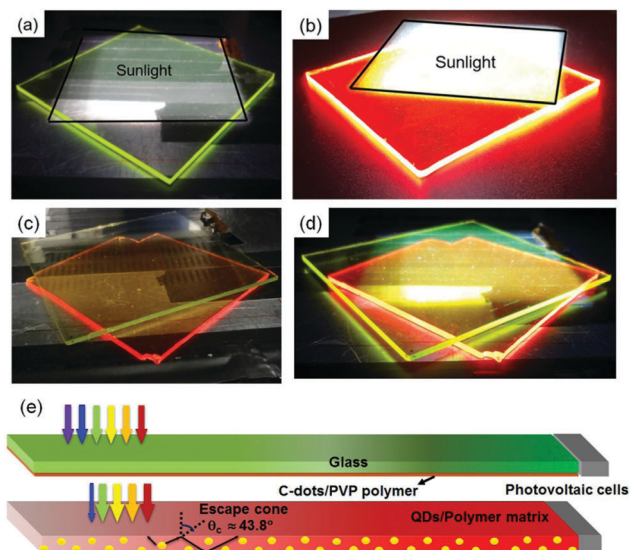

Fig. 3 (a) Absorption and PL spectra of the C-dots in methanol and in a PVP polymer thin film, respectively. The excitation wavelength is λ_{ex} = 350 nm. (b) Absorption and PL spectra of the CdSe/CdS QDs in toluene and in a PLMA polymer matrix, respectively. The excitation wavelength is λ_{ex} = 444 nm.

of the LSCs based on the QDs are 10×10 cm^2. No obvious variation can be found in the absorption and emission spectra before and after incorporation of the QDs into the polymer matrix (Fig. 3b). The CdSe/CdS QDs exhibit a large Stokes shift ($\sim$500 meV) due to the delocalization of electrons in the shell region, which is a typical behavior in "giant" QDs.[21,22] As reported in our previous work, before and after transferring the QDs or C-dots from the solution phase into the PLMA or PVP polymer, there are no significant changes of PL QY for the investigated samples, as confirmed by the PL decay measurement.[19,20,23]

As shown in Fig. 4a, the C-dot based LSC exhibits very good transparency in the range of 500 to 700 nm (transmittance >82%). The square large-area LSC ($0.2 \times 10 \times 10$ cm^3) appears semi-transparent and a clear concentrated yellow or red light can be seen from the edges under one simulated sun illumination (100 mW cm^{-2}) (Fig. 4a–c) or under room light (Fig. 4d). As shown in Fig. 4e, the thin film based on the C-dots is placed on the top-surface of the LSC based on the QDs. The LSCs (dimension: $0.2 \times 10 \times 10$ cm^3) were illuminated perpendicular to their surface using an AM 1.5G solar simulator (100 mW cm^{-2}). An optical power meter was coupled with one edge of the LSC and the emitted light intensity on the edge was measured. No significant difference can be found in the external optical efficiencies measured using the silicon solar cell or optical power meter.[23] The LSC based on the C-dots shows an η of 0.7% (Table 1 and Table S1, ESI†). The LSC based on the CdSe/CdS QDs show an η of 1.2% under one sun illumination (Table 1 and Table S1, ESI†), similar to the reported value with a similar area.[22,23] In the tandem-structured LSC based on the C-dots and QDs (Fig. 4c and d), the first layer LSC based on the C-dots shows an η of 0.7%. The second layer LSC based on the QDs shows an η of 0.7%, resulting in an overall η of 1.4% (Table 1). The decrease of the η of the QD based LSC after placing the C-dot thin film on its top is due to the decrease of the absorption of sunlight.[19] In this system, there is a strong overlap of the absorption between the C-dots and the CdSe/CdS QDs (Fig. 3).

This journal is © The Royal Society of Chemistry 2018

J. Mater. Chem. C, 2018, 6, 10059–10066 | 10063

Fig. 4 (a and b) Photographs of the single LSCs comprising C-dots (a) and CdSe/CdS QDs (b) under one sun illumination (100 mW cm^{-2}). (c and d) Photographs of the tandem LSCs comprising C-dots (top layer) and CdSe/CdS QDs (bottom layer) under ambient conditions (c) and one sun illumination (d). LSC dimensions: $10 \times 10 \times 0.2$ cm^3. (e) Schematic diagram of a typical tandem LSC configuration with a top layer of LSC based on C-dot/polymer spin-coated on a glass substrate and a bottom layer of LSC by incorporating QDs into a polymer matrix.

The first layer based on the C-dots could reflect the sunlight and decrease the efficient absorption of the QD layer. In future, one would select C-dots that only absorb UV light and exhibit a small absorption overlap with QDs in order to further improve the efficiency of tandem LSCs. The higher overall η compared to that of a single-layer LSC may benefit from both the efficient absorption of sunlight by both C-dots and QDs and the decrease in energy loss due to the escaped emitted light,[19] as the escaped emission (less than 500 nm) from the C-dot film can be partially reabsorbed by the QDs in the bottom layer.

3.3. Stability of the LSC based on the CdSe/CdS QDs

In general, colloidal bare QDs such as PbS or CdSe are more sensitive to UV light.[19,20,23] UV induced surface oxidation or chemical degradation of QDs is a common reason for the decrease of PL QY.[25] This decrease could be suppressed by using core/shell structured QDs.[21,22] For instance, the photo-stability of core/shell QDs can be largely improved compared to that of bare QDs, as the shell can isolate the core QDs from surrounding chemical environments.[38] Typically, the band

Table 1 External optical efficiencies for the single-layer and tandem LSCs based on C-dots and CdSe/CdS QDs under one sun illumination (100 mW cm^{-2}). The PL QY values of the C-dots and CdSe/CdS QDs in solution are included

LSCs	QDs	PL QY (%)	η (%)
Single	C-dots	40 ± 5	0.7 ± 0.1
Single	CdSe/CdS QDs	50 ± 5	1.2 ± 0.1
Tandem	C-dots	40 ± 5	0.7 ± 0.1
	CdSe/CdS QDs	50 ± 5	0.7 ± 0.1

energy level in core/shell "giant" QDs (e.g. CdSe/CdS core/thick shell QDs[21,22]) used as highly emissive emitters for LSCs is a quasi type II structure in which the electrons are delocalized across the entire QD volume, but the holes are still confined in the core region.[22] The leakage of electrons leads to the special separation of the electron–hole pair and induces a large Stokes shift in core/shell QDs, such as CdSe/CdS.[22] However, electrons in the core/shell QDs can still leak into the surface of the QDs, further quenched by the surrounding chemicals, which leads to a decrease of the PL QY, especially after exposure to UV light. As shown in Fig. 5a, upon exposure to a high dose of UV illumination (400 nm light emitting device with an intensity of 1.3 W cm^{-2}, equal to 260 sun illumination[7]), after 10 h illumination, over 95% of the integrated PL intensity is retained for the QD based LSC and 100% for the LSC based on C-dots. After 70 h UV illumination, the integrated PL intensity of the LSC based on QDs remains only 43% of its initial value. It is well known that PL quenching due to uncontrolled aggregation can result in a decrease of the PL intensity. However, for the core/shell QDs, the quenching efficiency decreases as the shell thickness increases due to the reduced spectral overlap between the absorption and emission.[53] Considering the relatively small spectral overlap, the large decrease in the PL intensity of the LSCs based on the QDs may be due to the UV-induced surface defects, which serve as surface recombination centers for photo-generated excitons.[19] By placing the C-dot thin film on the top of the LSC based on the QDs, the integrated PL intensity remains 75% of its initial value after 70 h illumination, which is 1.7 times higher than that of the LSC without a C-dot layer (43% of its initial value). This improvement is due to the efficient absorption of C-dots, which decrease the UV dose (50% of initial dose) on the surface of the LSC based on the CdSe/CdS QDs. As shown in Fig. 5b, the integrated PL intensity of the LSC based on C-dots remains 50% of its initial value. However, there is no significant variation of the absorption spectra of the C-dots before and after UV illumination. The stable absorption spectrum of the C-dots indicates that the structure of the C-dots is stable during the UV illumination. In addition, before and after the UV illumination, the PL peak position of the C-dots or QDs does not show a significant variation. Thus, the decrease of the PL intensity of the LSC based on the C-dots is mainly attributed to the PL quenching because of the surface-traps. It is worth emphasizing that the stable absorption spectrum of the C-dots under UV light endows efficient protection for the LSC based on the CdSe/CdS QDs.

To further understand the PL quenching mechanism in LSCs after UV illumination, we measured the fluorescence decay of the LSCs. The C-dot-based LSC was placed on the top of the LSC based on the QDs. After 70 h UV illumination, as shown in Fig. 5c, the CdSe/CdS QDs exhibit a typical lifetime of 45 ± 1 ns, which is lower than their initial lifetime (50 ± 1 ns) before UV illumination. Consistently, the lifetime of the C-dots also presents a decrease after UV illumination, from 7 ± 0.5 ns to 5 ± 0.5 ns (Fig. 5d). The decrease in the lifetime indicates that the PL quenching in the QDs or C-dots is due to the non-radiative recombination of excitons through the recombination
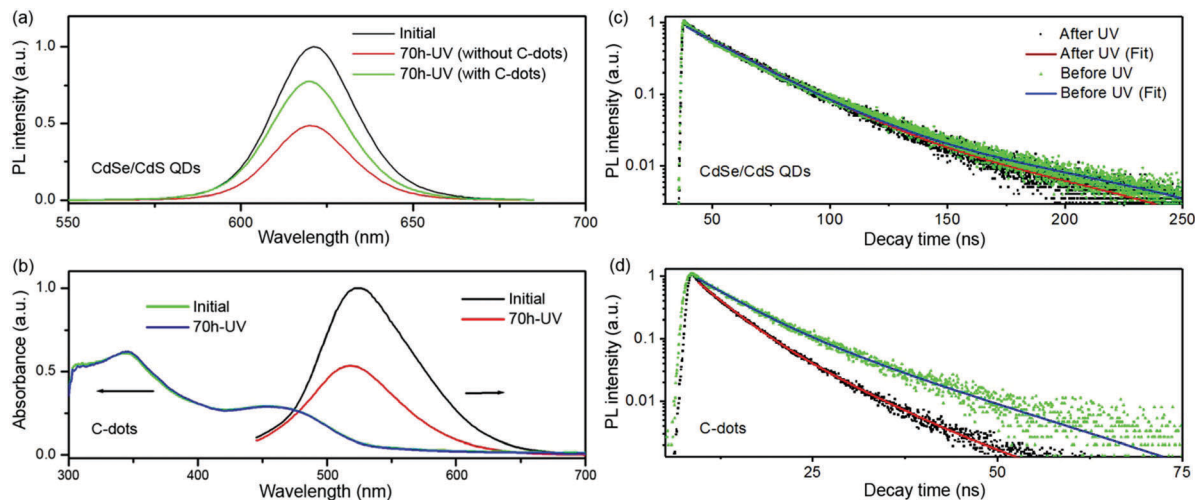
Fig. 5 (a) PL spectra of the LSCs based on CdSe/CdS QDs before and after 70 h UV illumination under ambient conditions with or without a protective layer based on C-dot/PVP. (b) Absorption and PL spectra of the LSCs based on C-dots before and after 70 h UV illumination under ambient conditions. (c and d) PL decay curves of the CdSe/CdS QDs (c) and C-dots (d) before and after 70 h UV illumination. The excitation wavelength is λ_{ex} = 444 nm for the CdSe/CdS QDs and λ_{ex} = 350 nm for the C-dots.

centers, other than the photo-bleaching or photo-oxidation, which often leads to the blue- or red-shift of the PL peak position.[37,38] Thus, the PL stability can be improved by modifying their surface to isolate the quenchers around the C-dots.

Furthermore, we estimated the cost of C-dots and CdSe/CdSe QDs by considering the cost of precursors used in the synthesis. The cost for one gram CdSe/CdS QDs is around 15 $, which is consistent with the estimated cost (10 $ per g) for a similar type of core/shell QD by Klimov *et al.*[30] The cost of C-dots is around 1 $ per g, which is 10-fold cheaper than that of CdSe/CdS QDs. Thus, we propose to use the low-cost C-dots as a sacrificial agent, protecting the LSC based on inorganic QDs against UV illumination. This strategy may also be applied for LSCs based on other types of inorganic QDs, such as Si, PbS/CdS, and perovskite QDs. Future work may focus on the optimization of the concentration of C-dots, the enhancement of the photo-stability of the C-dots[40] and the selection of types of inorganic QDs to improve the performance of LSCs.

4. Conclusions and perspectives

In conclusion, we have demonstrated improved long-term stability of large-area colloidal QD based LSCs by using a C-dot based thin film as a protective layer. The as-fabricated semi-transparent tandem structured device exhibits an external optical efficiency of $\sim$1.4% under one sunlight illumination (100 mW cm^{-2}), which is a 16% increase in efficiency over the LSC based on CdSe/CdS QDs. The presence of C-dots can dramatically enhance the long-term photo-stability of LSC devices based on QDs. Upon 70 h UV illumination, the QD based LSC with the C-dot thin film retains 75% of its initial integrated PL intensity, which is 1.8 times higher than that of the LSC without a C-dot layer. This finding indicates that C-dots can be used as an efficient UV absorber to improve the long-term photo-stability of LSCs based on colloidal QDs.

This methodology can be used to improve the long-term photo-stability of optoelectronic devices based on QDs, such as QD solar cells and other types of tandem LSCs based on perovskites and quantum wells or organic dyes and polymers.

Conflicts of interest

The authors declare no competing financial interests.

Acknowledgements

References

1 H. Zhao and F. Rosei, *Chem*, 2017, **3**, 229–258.
2 U. Bach, D. Lupo, P. Comte, J. E. Moser, F. Weissörtel, J. Salbeck, H. Spreitzer and M. Grätzel, *Nature*, 1998, **395**, 583–585.
3 G. Selopal, H. Zhao, X. Tong, D. Benetti, F. Navarro-Pardo, Y. Zhou, D. Barba, F. Vidal, Z. Wang and F. Rosei, *Adv. Funct. Mater.*, 2017, **27**, 1701468.
4 M. A. Green, K. Emery, Y. Hishikawa and W. Warta, *Prog. Photovolt: Res. Appl.*, 2010, **18**, 346–352.
5 B. A. Andersson, C. Azar, J. Holmberg and S. Karlsson, *Energy*, 1998, **23**, 407–411.

This journal is © The Royal Society of Chemistry 2018

J. Mater. Chem. C, 2018, **6**, 10059–10066 | **10065**

6   A. Feltrin and A. Freundlich, *Renewable Energy*, 2008, **33**, 180–185.

7   W. Wang, Y. W. Su and C. H. Chang, *Sol. Energy Mater. Sol. Cells*, 2011, **95**, 2616–2620.

8   A. Rockett and R. W. Birkmire, *J. Appl. Phys.*, 1991, **70**, R81–R97.

9   A. Louwen, W. Sark, R. Schropp and A. Faaij, *Sol. Energy Mater. Sol. Cells*, 2016, **147**, 295–314.

10 M. Park, S. H. Lee, D. Kim, J. Kang, J. Y. Lee and S. M. Han, *ACS Appl. Mater. Interfaces*, 2018, **10**, 7214–7222.

11 B. A. Gonfa, H. Zhao, J. Li, J. Qiu, M. Saidani, S. Zhang, R. Izquierdo, N. Wu, M. A. El Khakani and D. Ma, *Solar Energy Mater. Sol. Cells*, 2014, **124**, 67–74.

12 D. Wang, J. K. Baral, H. Zhao, B. A. Gonfa, V. V. Truong, M. A. Elkhakani, R. Izquierdo and D. Ma, *Adv. Funct. Mater.*, 2011, **21**, 4010–4018.

13 Z. Du, Z. Pan, F. Fabregat-Santiago, K. Zhao, D. Long, H. Zhang, Y. Zhao, X. Zhong, J. S. Yu and J. Bisquert, *J. Phys. Chem. Lett.*, 2016, **7**, 3103–3111.

14 G. H. Kim, F. P. García de Arquer, Y. J. Yoon, X. Lan, M. Liu, O. Voznyy, Z. Yang, F. Fan, A. H. Ip, P. Kanjanaboos, S. Hoogland, J. Y. Kim and E. H. Sargent, *Nano Lett.*, 2015, **15**, 7691–7696.

15 H. Tan, A. Jain, O. Voznyy, X. Z. Lan, F. P. García de Arquer, J. Z. Fan, R. Quintero-Bermudez, M. J. Yuan, B. Zhang, Y. C. Zhao, F. J. Fan, P. C. Li, L. N. Quan, Y. B. Zhao, Z. H. Lu, Z. Y. Yang, S. Hoogland and E. H. Sargent, *Science*, 2017, **355**, 722–726.

16 A. Goetzberger and W. Greubel, *Appl. Phys.*, 1977, **14**, 123–139.

17 L. H. Slooff, E. E. Bende, A. R. Burgers, T. Budel, M. Pravettoni, R. P. Kenny, E. D. Dunlop and A. Büchtemann, *Phys. Status Solidi RRL*, 2008, **2**, 257–259.

18 M. G. Debije and P. P. C. Verbunt, *Adv. Energy Mater.*, 2012, **2**, 12–35.

19 Y. Zhou, D. Benetti, X. Tong, L. Jin, Z. M. Wang, D. Ma, H. Zhao and F. Rosei, *Nano Energy*, 2018, **44**, 378–387.

20 Y. Zhou, D. Benetti, Z. Fan, H. Zhao, D. Ma, A. O. Govorov, A. Vomiero and F. Rosei, *Adv. Energy Mater.*, 2016, **6**, 1501913.

21 I. Coropceanu and M. G. Bawendi, *Nano Lett.*, 2014, **14**, 4097–4101.

22 F. Meinardi, A. Colombo, K. A. Velizhanin, R. Simonutti, M. Lorenzon, L. Beverina, R. Viswanatha, V. I. Klimov and S. Brovelli, *Nat. Photonics*, 2014, **8**, 392–399.

23 H. Zhao, D. Benetti, L. Jin, Y. F. Zhou, F. Rosei and A. Vomiero, *Small*, 2016, **12**, 5354–5365.

24 C. S. Erickson, L. R. Bradshaw, S. McDowall, J. D. Gilbertson, D. R. Gamelin and D. L. Patrick, *ACS Nano*, 2014, **8**, 3461–3467.

25 H. Li, K. Wu, J. Lim, H. J. Song and V. I. Klimov, *Nat. Energy*, 2016, **1**, 16157.

26 F. Meinardi, H. McDaniel, F. Carulli, A. Colombo, K. A. Velizhanin, N. S. Makarov, R. Simonutti, V. I. Klimov and S. Brovelli, *Nat. Nanotechnol.*, 2015, **10**, 878–885.

27 F. Meinardi, S. Ehrenberg, L. Dhamo, F. Carulli, M. Mauri, F. Bruni, R. Simonutti, U. Kortshagen and S. Brovelli, *Nat. Photonics*, 2017, **11**, 177–185.

28 V. Wittwer, W. Stahl and A. Goetzberger, *Sol. Energy Mater.*, 1984, **11**, 187–197.

29 L. Desmet, A. J. M. Ras, D. K. G. de Boer and M. G. Debijie, *Opt. Lett.*, 2012, **37**, 3087–3089.

30 K. Wu, H. Li and V. I. Klimov, *Nat. Photonics*, 2018, **12**, 105–110.

31 G. Griffini, L. Brambilla, M. Levi, M. D. Zoppo and S. Turri, *Sol. Energy Mater. Sol. Cells*, 2013, **111**, 41–48.

32 G. Griffini, M. Levi and S. Turri, *Sol. Energy Mater. Sol. Cells*, 2013, **118**, 36–42.

33 A. Kaniyoor, B. McKenna, S. Comby and R. C. Evans, *Adv. Opt. Mater.*, 2016, **4**, 444–456.

34 I. Meazzini, N. Willis-Fox, C. Blayo, J. Arlt, S. Clément and R. C. Evans, *J. Mater. Chem. C*, 2016, **4**, 4049–4059.

35 M. Sharma, K. Gungor, A. Yeltik, M. Olutas, B. Guzelturk, Y. Kelestemur, T. Erdem, S. Delikanli, J. R. McBride and H. V. Demir, *Adv. Mater.*, 2017, **29**, 1700821.

36 H. Zhao, Y. Zhou, D. Benetti, D. Ma and F. Rosei, *Nano Energy*, 2017, **37**, 214–223.

37 H. Zhao, D. Wang, M. Chaker and D. Ma, *J. Phys. Chem. C*, 2011, **115**, 1620–1626.

38 H. Zhao, D. Wang, T. Zhang, M. Chaker and D. Ma, *Chem. Commun.*, 2010, **46**, 5301–5303.

39 S. Zhu, Q. Meng, L. Wang, J. Zhang, Y. Song, H. Jin, K. Zhang, H. Sun, H. Wang and B. Yang, *Angew. Chem., Int. Ed.*, 2013, **52**, 3953–3957.

40 Y. Liu, L. Zhou, Y. Li, R. Deng and H. Zhang, *Nanoscale*, 2017, **9**, 491–496.

41 S. N. Qu, D. Zhou, D. Li, W. Ji, P. Jing, D. Han, L. Liu, H. Zeng and D. Shen, *Adv. Mater.*, 2016, **28**, 3516–3521.

42 Z. Xie, F. Wang and C. Y. Liu, *Adv. Mater.*, 2012, **24**, 1716–1721.

43 P. Zhang, W. Li, X. Zhai, C. Liu, L. Dai and W. Liu, *Chem. Commun.*, 2012, **48**, 10431–10433.

44 B. Chen and J. Feng, *J. Phys. Chem. C*, 2015, **119**, 7865–7872.

45 Y. Wang, Z. Yin, Z. Xie, X. Zhao, C. Zhou, S. Zhou and P. Chen, *ACS Appl. Mater. Interfaces*, 2016, **8**, 9961–9968.

46 J. Liu, Z. Xie, Y. Shang, J. Ren, R. Hu, B. Guan, J. Wang, T. Ikeda and L. Jiang, *ACS Appl. Mater. Interfaces*, 2018, **10**, 6701–6710.

47 Y. Li, P. Miao, W. Zhou, X. Gong and X. Zhao, *J. Mater. Chem. A*, 2017, **5**, 21452–21459.

48 S. Qu, X. Wang, Q. Lu, X. Liu and L. Wang, *Angew. Chem., Int. Ed.*, 2012, **51**, 12215–12218.

49 G. Griffini, M. Levi and S. Turri, *Renewable Energy*, 2015, **78**, 288–294.

50 R. W. Olson, R. F. Loring and M. D. Fayer, *Appl. Opt.*, 1981, **20**, 2934–2940.

51 L. R. Wilson, B. C. Rowan, N. Robertson, O. Moudam, A. C. Jones and B. S. Richards, *Appl. Opt.*, 2010, **49**, 1651–1661.

52 S. Tsoi, D. J. Broer, C. W. M. Bastiaansen and M. G. Debijie, *Opt. Express*, 2010, **18**, A536–A543.

53 T. Kang, K. Um, J. Park, H. Chang, D. C. Lee, C. K. Kim and K. Lee, *Sens. Actuators, B*, 2016, **222**, 871–878.